REVIEWS

Journal of Semiconductors
(2019) 40, 081506
doi: 10.1088/1674-4926/40/8/081506

Progress on microscopic properties of diluted magnetic semiconductors by NMR and μSR

Yilun Gu[1], Shengli Guo[1], and Fanlong Ning[1, 2, †]

[1]Zhejiang Province Key Laboratory of Quantum Technology and Device and Department of Physics, Zhejiang University, Hangzhou 310027, China

[2]Collaborative Innovation Center of Advanced Microstructures, Nanjing University, Nanjing 210093, China

Abstract: Diluted magnetic semiconductors (DMSs) that possess both properties of semiconductors and ferromagnetism, have attracted a lot of attentions due to its potential applications for spin-sensitive electronic devices. Recently, a series of bulk form DMSs isostructural to iron-based superconductors have been reported, which can be readily investigated by microscopic experimental techniques such as nuclear magnetic resonance (NMR) and muon spin rotation (μSR). The measurements have demonstrated that homogeneous ferromagnetism is achieved in these DMSs. In this review article, we summarize experimental evidences from both NMR and μSR measurements. NMR results have shown that carriers facilitate the interactions between distant Mn atoms, while μSR results indicate that these bulk form DMSs and (Ga,Mn)As share a common mechanism for the ferromagnetic exchange interactions.

Key words: diluted magnetic semiconductors; muon spin rotation; nuclear magnetic resonance; ferromagnetism

Citation: Y L Gu, S L Guo, and F L Ning, Progress on microscopic properties of diluted magnetic semiconductors by NMR and μSR[J]. *J. Semicond.*, 2019, 40(8), 081506. http://doi.org/10.1088/1674-4926/40/8/081506

1. Introduction

Ferromagnetic semiconductors possess both properties of semiconductors and ferromagnetism, which have attracted many attentions due to their potential applications for spin-sensitive electronic devices[1]. In past, scientists mainly focused on two research streams of ferromagnetic semiconductors: one is the concentrated magnetic semiconductors where magnetic atoms locate in each unit cell, for example, EuO[2] and $CdCr_2S_4$[3]; the other one is diluted magnetic semiconductors (DMSs) in which small amount of magnetic atoms have been doped into non-magnetic semiconductors and magnetic ordering has developed. In 1980s, Mn doped II–VI semiconductors, such as (Zn,Mn)Se[4], (Zn,Mn)Te[5], (Cd,Mn)Se[6] and (Cd,Mn)Te[7], etc. have been widely investigated. The difficulty encountered in II–VI DMSs is the low carrier concentrations, which prevents the formation of ferromagnetic long range ordering.

In 1990s, the research on DMSs has been focusing on III–V DMSs. Among them, (Ga,Mn)As has been the most thoroughly investigated system[8–11]. As of today, the highest Curie temperature in (Ga,Mn)As has been reported as ~200 K[12–14]. In (Ga,Mn)As, Mn substitution for Ga introduces both spins and carriers simultaneously, which makes it difficult to control individual concentrations of spins and carriers, respectively. On the other hand, the mismatch valences of Mn^{2+} and Ga^{3+} limits the solid solution and only metastable (Ga,Mn)As films can be synthesized by MBE (molecular beam epitaxy) method. More progresses of III–V DMSs can be found in a recent review article by Tanaka *et al.*[15].

Correspondence to: F L Ning, ningfl@zju.edu.cn
Received 3 JUNE 2019; Revised 8 JULY 2019.

Recently, a series of novel bulk form DMSs isostructural to iron-based superconductors have been reported. They are 111-type Li(Zn,Mn)P[16] and Li(Zn,Mn)As[17], 1111-type (La,Ba)(Zn,Mn)AsO[18], and 122-type (Ba,K)$(Zn,Mn)_2As_2$[19] and $Ba(Zn,Co)_2As_2$[20], etc. In (Ba,K)$(Zn,Mn)_2As_2$, the highest Curie temperature T_C has been reported as high as 230 K [21]. While in $Ba(Zn,Co)_2As_2$, ferromagnetic ordering below 45 K with n-type carriers has been achieved[20]. Furthermore, these bulk form DMSs have the advantages of decoupled charge and spin doping, and each concentration can be precisely controlled. The characterization and macroscopic properties have been summarized in a recent review article by Guo *et al.*[22]. On the other hand, with the bulk form specimens, nuclear magnetic resonance (NMR) and muon spin rotation/relaxation/resonance (μSR) experimental techniques can be applied, and some microscopic information by two techniques can be readily provided. In this review article, we will summarize the unique information obtained from both NMR and μSR measurements on these DMSs materials. Our results will shed light on understanding the general mechanism of ferromagnetic long range ordering in DMSs.

2. Microscopic methods

NMR and μSR are powerful to measure spin dynamics and magnetic excitations in magnetically ordered systems. However, each experimental probe has its own requirements for samples. For NMR, the testing sample is usually needed to be put into a cylindrical coil, and signal to noise (S/N) ratio is largely relying on the filling factor of samples into the coil. S/N ratio is very small for film specimens, which makes it very hard to measure (Ga,Mn)As and other film specimens. While for μSR, bulk samples are also preferred. Thanks to the development of technology at Paul Scherrer Institute, it is now possible to measure films with thickness of tens of nanometers by

low energy muons.

2.1. NMR

NMR is a local, site-selective probe. It is powerful to measure both static and dynamic susceptibilities. Due to the combinations of nucleons, some nuclei have certain nuclear spin S. The energy levels for a non-zero nuclear spin S will split under an external magnetic field due to the Zeeman effect. To get a resonance, an alternating field is applied perpendicular to the external magnetic field. When the frequency of the alternating field is appropriate, a resonance takes place between different energy levels. In practice, we need to choose nuclei with good sensitivity and large natural abundance to acquire reasonable S/N ratio. Nuclear spins interact with electrons via dipole-dipole interactions, Fermi's contact interactions (for s- electrons), and electron's orbital motion. Through the shift of resonance frequencies, we can obtain the static susceptibility, which is called Knight shift. Knight shift contains two parts, one is the orbital part which arises from the electron's orbital motion. This part is temperature independent, and is called chemical shift. The second part is the spin susceptibility, which satisfies the formula $K = (A_0/g\mu_{\rm B})\chi_{\rm spin}$, where $A_0/g\mu_{\rm B}$ is the hyperfine coupling constant. When both Knight shift (K) by NMR and bulk susceptibility (χ) by SQUID (superconducting quantum interference device) are available, a plot with K versus χ can be conducted. The slope will give the magnitude of $A_0/g\mu_{\rm B}$ directly. NMR can also provide the information of spin dynamics and the strength of magnetic fluctuations through the measurement of nuclear spin-lattice relaxation rate, $1/T_1$. Usually an 180 degree pulse is applied to flip the polarized nuclear spin. After removing the pulse, nuclear spins will get back to the thermally equilibrium state. This process can take several minutes in some non-magnetic semiconductors, but only several milliseconds in some correlated systems, such as diluted magnetic semiconductors. This process is also affected by the crystal field environment. $1/T_1$ therefore provides important information of the electron correlations and interactions.

The spin contribution to $1/T_1$ may be written using the imaginary part of the dynamical electron spin susceptibility $\chi''(\boldsymbol{q}, f_0)$

$$\frac{1}{T_1} \propto T\sum_q |A(\boldsymbol{q})|^2 \frac{\chi''(\boldsymbol{q}, \boldsymbol{f}_0)}{\boldsymbol{f}_0} \quad , \tag{1}$$

where $A(\boldsymbol{q})$ is the hyperfine form factor, and f_0 is the resonance frequency.

Using the Gaussian approximation for the spin-spin correlation function, we can express

$$\frac{1}{T_1} = \sqrt{2\pi}\frac{S(S+1)}{3\omega_{\rm e}}\left(\frac{A_0}{\hbar}\right)^2 \quad , \tag{2}$$

where

$$\omega_{\rm e}^2 = \frac{2}{3}zS(S+1)\left(\frac{J}{\hbar}\right)^2 \quad , \tag{3}$$

and z is the number of Mn sites within the range of Mn–Mn interactions for the case of Li(Zn,Mn)P and Li(Cd,Mn)P discussed in the following.

2.2. μSR

μSR is another powerful method to investigate DMSs. Due to the parity breaking, muons are nearly 100% polarized even without the application of an external field. After stopping in the sample muons begin to precess in the local field. By measuring the anisotropic distribution of the positrons emitted by muons, we can infer the internal magnetic environment around muons. μSR is a high field-sensitive method and we can obtain volume fraction of magnetic ordered state using zero field (ZF-) μSR and weak transverse field (wTF-) μSR methods. For the analysis of the ZF μSR time spectra in DMS system, we usually use a two-component function. We write the function as

$$A(t) = A_{\rm mag}G_Z^L(t) + A_{\rm para}\exp\left[-(\lambda t)^\beta\right] \quad . \tag{4}$$

The first term on the right hand side represents the magnetic component, and the second term represents the paramagnetic component, where β is a temperature-independent constant, and G_Z^L is the relaxation function for a static magnetic field with Lorentzian distribution:

$$f(H_i) = \frac{\gamma_\mu}{\pi}\frac{a}{a^2+\gamma_\mu^2 H_i^2} \quad , \tag{5}$$

where $\gamma_\mu = 2\pi\times 1.3554\times 10^4\ {\rm s}^{-1}{\rm G}^{-1}$ is the gyromagnetic ratio of muon, and a/γ_μ represents a field amplitude for the half-width at half-maximum, and G_Z^L satisfies the formula:

$$G_Z^L(T) = \frac{1}{3} + \frac{2}{3}(1-at)\exp(-at) \quad , \tag{6}$$

as observed in diluted-alloy and spin glasses. The series expansion for Eq. (6) in terms of at is

$$G_Z^L(T) = 1 - \frac{4}{3}at + a^2t^2 + \cdots . \tag{7}$$

The series expansion for an exponential decay function $G_Z(t) = \exp(-\Lambda t)$ is

$$G_Z^L(T) = 1 - \Lambda t + \frac{1}{2}\Lambda^2 t^2 + \cdots , \tag{8}$$

which was employed for the analysis of ZF-μSR spectra in (Ga,Mn)As[23]. Comparing the Eqs. and (8), we notice that Λ is identical to $\frac{4}{3}a$. Then we can get the static local field parameter $a_{\rm s}$ by analysing $G_Z^L(t)$, which gives the information about the ferromagnetic ordering. Besides, longitudinal field (LF-) μSR also gives us information about spin dynamics.

3. NMR and μSR results of DMSs

3.1. 111-system

Masek *et al.* firstly predicted that I–II–V Li(Zn,Mn)As could become a new diluted magnetic semiconductor[24]. In 2011, Deng *et al.* successfully synthesized the samples and observed ferromagnetic ordering below the Curie temperature ~ 50 K[17]. LiZnAs has a similar cubic crystal structure to that of GaAs. Doping Mn into Zn sites could be as high as 10%. In Fe-based superconductor family, LiFeAs is named as 111-type ac-

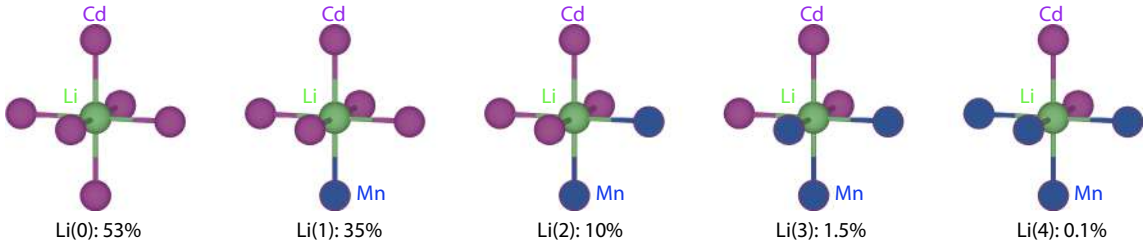

Fig. 1. (Color online) The probability to find Li(0), Li(1), Li(2), Li(3), Li(4) for 10% Mn doped into Cd sites in LiCdP. The number in bracket means the number of Mn atoms at N.N. Cd sites.

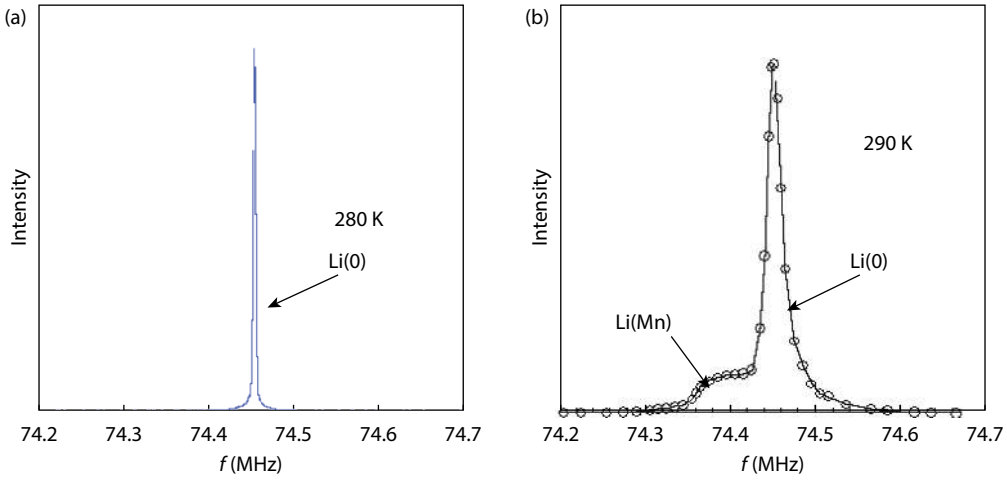

Fig. 2. (Color online) The representative ^{7}Li line shapes of (a) $Li_{1.1}CdP$ and (b) $Li_{1.1}(Cd,Mn)P$.

cording to the chemical formula. For convenience, we also name Li(Zn,Mn)As as 111-type DMS. This family includes four other members, Li(Zn,Mn)P[16], Li(Cd,Mn)P[25], Li(Zn,Cr)As[26] and Li(Zn,Mn,Cu)As[27]. They all have the cubic crystal structure [16, 17, 25–27].

3.1.1. NMR

As explained above, we need to choose a proper nucleus for conducting successful NMR experiment. Our initial attempt was to measure NMR signal from phosphorus in Li(Zn,Mn)P since P has a nuclear spin 1/2 and the measurement should have been easier. Unfortunately, the p-orbital of P atoms strongly hybridize with d-orbital of Mn atoms, which induces a very broad NMR lineshape especially below the Curie temperature. We then switched to measure Li NMR. Li has a nuclear spin 3/2, which should have given rise to three NMR lines if the charge distribution of nuclei is deformed from a spherical shape. This is because the nuclear quadrupole moment will interact with electric field gradient of the charge environment, which shifts the Zeeman levels. However, in LiCdP, as can be seen from the first picture in Fig. 1, six Cd atoms sit at nearest neighbor (N.N) sites of Li atoms. This means that no quadrupole interaction and only one NMR line exist, as shown in Fig. 2(a). This Li line is named as Li(0) site since no Mn is doped yet. But once Mn atoms are doped, the situation changes. For each Li atom, it can have zero, 1 to 6 Mn atoms at its nearest neighbor sites. We show five different possibilities in Fig. 1. Doping Mn directly changes the line shape of Li. As can be seen from Fig. 2(b), a broad hump appears at the left hand side of Li(0) site. This hump is from Li atoms with 1–6 Mn atoms at its N.N. sites, and is defined as Li(Mn) sites. Li(Mn) sites include Li(0), Li(1), Li(2), Li(3), Li(4), Li(5) and Li(6) sites as depicted in Fig. 1. Focusing on the shifts of Li(0) and Li(Mn) sites, we can readily obtain the static susceptibilities for each of them.

In a similar way, Ding *et al.* conducted the NMR measurements on Li(Zn,Mn)P that has the maximum Curie temperature ~ 34 K[16]. In Fig. 3, we show the results of $Li(Zn_{0.9}Mn_{0.1})P$ (adopted from Ref. [28]). We measured the Knight shift and $1/T_1$ of ^{7}Li nuclear spins. Identical to the convention in Li(Cd,Mn)P shown in Fig. 1 and Fig. 2, Li(0) represents Li atoms that have no Mn at nearest neighbour Zn sites, and Li(Mn) are Li atoms that have 1–6 Mn atoms at nearest neighbour Zn sites. The half-height-frequency-width (HHFW) of Li(0) have the same temperature dependence with the Knight shift of Li(Mn), which indicates that they are electronically coupled, and Mn-Mn interaction extends over the whole sample. This result is consistent with μSR results that ferromagnetism is intrinsic and homogeneous[29]. In Fig. 3(b), we show the relaxation rate $1/T_1$ of Li(0) and Li(Mn). $1/T_1$ of Li(Mn) reaches ~ 400 s^{-1} above T_C and is almost 50 times lager than that of Li(0). At the temperature above $T_C \approx 25$ K, $1/T_1$ of Li(Mn) becomes a constant. It indicates that the spin fluctuations are locked above T_C and the typical Mn–Mn spin interaction energy scale $|J|$ is ~ 100 K. Quite differently, $1/T_1$ of Li(0) shows a linear relationship with temperature above T_C, following the Korringa process arising from the Fermi surface excitations of a small number of conducting carriers. With these experimental evidences, we can readily conclude that carriers facilitate the interactions between distant Mn atoms. These results explain why a ferromagnetic ordering can be formed with a relatively high T_C but such a low density of Mn atoms and carriers[28].

3.1.2. μSR

For 111-type DMS, we show μSR results of $Li_{1.1}(Zn_{0.95}$-

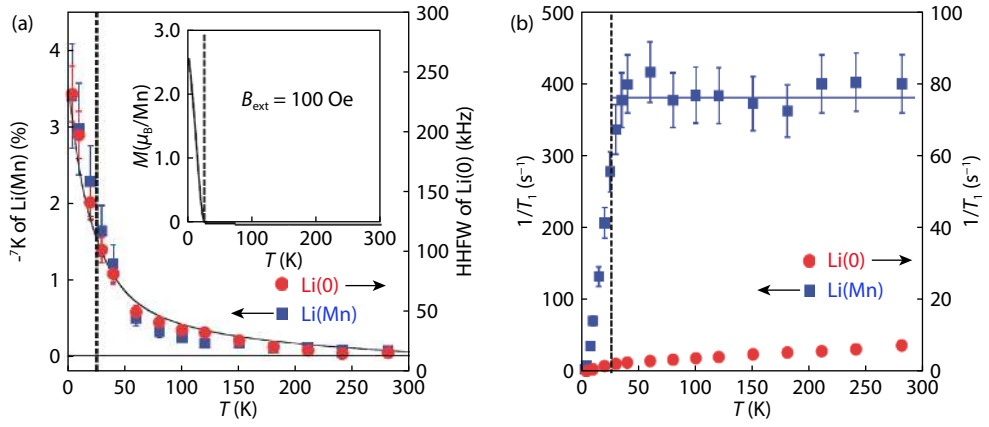

Fig. 3. (Color online) (a) The temperature dependence of the ^{7}Li NMR Knight shifts, $-^7K$, at the Li(Mn)sites. The HHFW of Li(0) in Li($Zn_{0.9}Mn_{0.1}$)P. Inset: The DC magnetization M measured at B_{ext} = 100 Oe. (b) $1/T_1$ of Li(0) and Li(Mn) of Li($Zn_{0.9}Mn_{0.1}$)P. The dashed line marks T_C = 25 K. Adopted from Ref. [28].

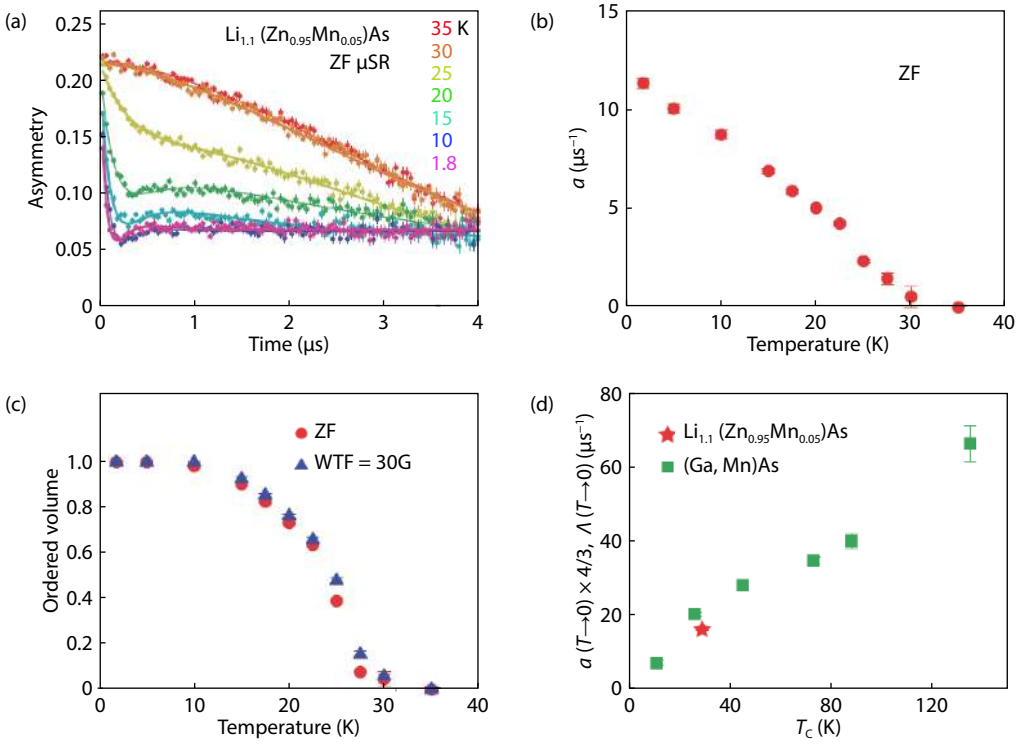

Fig. 4. (Color online) (a) The zero field μSR time spectra of $Li_{1.1}(Zn_{0.95}Mn_{0.05})As$. (b) The relaxation rate a of the signal that exhibits fast relaxation. (c) The volume fraction of the magnetically ordered region, derived from the amplitude of the fast relaxing signal. (d) Comparison between $Li_{1.1}(Zn_{0.95}Mn_{0.05})As$ and (Ga,Mn)As in a plot of the relaxation rate versus T_C. Adopted from Ref. [17].

$Mn_{0.05})As$ done by Deng *et al* in Fig. 4 (adopted from Ref. [17]). In Fig. 4(a), we show ZF-μSR time spectra of $Li_{1.1}(Zn_{0.95}Mn_{0.05})As$. Clearly, the time spectra exhibit an increase of the relaxation rate below $T \sim 25$ K. With the analysis discussed in Sec. 2, the temperature dependence of the relaxation rate can be deduced, and is shown in Fig. 4(b). The relaxation rate of ZF-μSR spectra starts to increase well below the Curie temperature $T_C \sim 29$ K. Following the analysis of two-component Eq. (4), we can obtain the magnetically ordered volume fraction and show it in Fig. 4(c). The ordered volume fraction starts to increase below T_C, and reaches 100 % below 10 K. This indicates that the ferromagnetism in Li(Zn,Mn)As has extend over the whole sample space, i.e., the ferromagnetism is homogenous and intrinsic. In Fig. 4(d), we show the comparison of static local field parameter a between $Li_{1.1}(Zn_{0.95}Mn_{0.05})As$ and (Ga,Mn)As with various Mn concentrations. All points fall into the same linear line, confirming that Li(Zn,Mn)As shares the same ferromagnetic mechanism with (Ga,Mn)As[17].

3.2. 1111-system

Following the research trend in Fe-based superconductors, we have also discovered a series of new materials named 1111-type DMSs. The first 1111-type DMS reported is (La,Ba)(Zn,Mn)AsO with T_C up to ~ 40 K[18], which has a tetragonal crystal structure with the space group $P4/nmm$, identical to LaFeAsO superconductors[30]. 1111-type DMS family also contains (La,Sr)(Zn,Mn)AsO[31], (La,Ca)(Zn,Mn)SbO[32], (Ba,K)F-(Zn,Mn)As[33] and (La,Sr)(Cu,Mn)SO[34]. They all have the tetra-

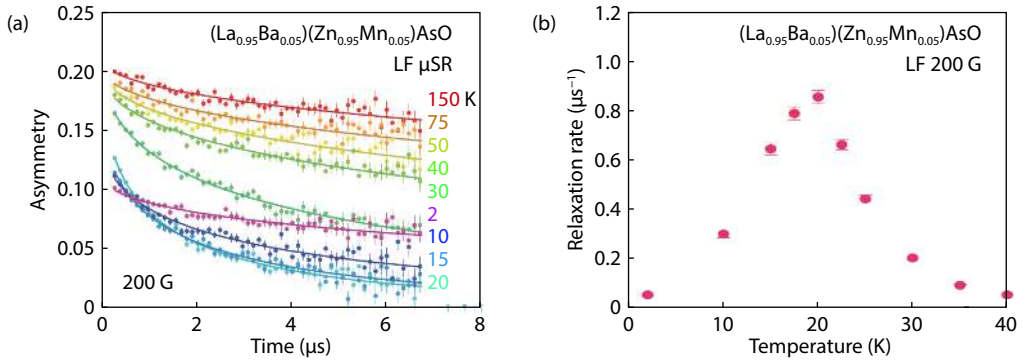

Fig. 5. (Color online) (a) The time spectra of LF-μSR in $(La_{0.95}Ba_{0.05})(Zn_{0.95}Mn_{0.05})AsO$ with a longitudinal field of 200 G. (b) Muon spin relaxation rate $1/T_1$ due to dynamic spin fluctuation. Adopted from Ref. [18].

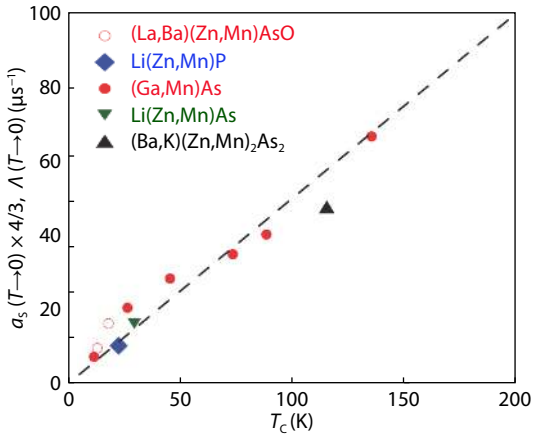

Fig. 6. (Color online) Correlation between the static internal field parameter a_s determined at 2 K by ZF-μSR versus Curie temperature T_C observed in (Ga,Mn)As, Li(Zn,Mn)As, Li(Zn,Mn)P, (La,Ba)(Zn,Mn)AsO and $(Ba,K)(Zn,Mn)_2As_2$. Adopted from Ref. [29].

gonal crystal structure, and are two-dimensional bulk form materials. The Curie temperature of (La,Sr)(Cu,Mn)SO reaches ~ 200 K, which is the highest T_C among 1111-type DMSs[34].

Ding *et al.* conducted μSR measurements on (La,Ba)(Zn,Mn)AsO. The result is shown in Fig. 5 (adopted from Ref. [18]). Below T_C, the time spectra of ZF-μSR show fast relaxation. The static local field parameter a_s obtained from the time spectra displays a similar temperature-dependence as that for Li(Zn,Mn)As and (Ga,Mn)As shown in Fig. 6, indicating that they share the same ferromagnetic mechanism. We have also conducted LF-μSR for $(La_{0.95}Ba_{0.05})(Zn_{0.95}Mn_{0.05})AsO$, and show the analysis of the time spectra in Fig. 5(a). The LF-μSR relaxation rate is obtained and shown in Fig. 5(b). It shows a clear peak at T ~ 20 K, consistent with the ZF-μSR results, which is the spin freezing temperature. It also agrees well with the results in DC magnetizations of (La,Ba)(Zn,Mn)AsO[18].

3.3. 122-system

Different from 111-system and 1111-system, the crystal structures of 122-type DMSs are not identical. The crystal structure of $(Ba,K)(Zn,Mn)_2As_2$ with T_C ~ 230 K iss tetragonal[21], while $(Ba,K)(Cu,Mn)_2Se_2$ with T_C ~ 18 K is orthorhombic[35] and $(Ca,Na)(Zn,Mn)_2As_2$ with T_C ~ 33 K is hexagonal[36]. Some 122-type DMSs also contain compounds with Cd atoms instead of Zn atoms, such as $(Sr,Na)(Cd,Mn)_2As_2$[37] and $(Ba,K)(Cd,Mn)_2As_2$[38]. They all have a hexagonal $CaAs_2Si_2$-type structure, similar to $(Ca,Na)(Zn,Mn)_2As_2$. The Curie temperature of $(Sr,Na)(Cd,Mn)_2As_2$ is ~ 13 K and that of $(Ba,K)(Cd,Mn)_2As_2$ is ~ 16 K.

Man *et al.* observed ferromagnetism in a new DMS $Ba(Zn,Mn,Co)_2As_2$ with n-type carriers[39], and they managed to obtain high quality polycrystal. Lately, $Ba(Zn,Co)_2As_2$ was confirmed by both Hall effect and Seebeck effect that the carriers are n-type. μSR measurements confirmed that the ferromagnetism in $Ba(Zn,Co)_2As_2$ is intrinsic and homogeneous[20]. The successful synthesis of n-type DMS is consistent with a theoretical prediction that n-type DMS may be realized in semiconductors with narrow band gaps[40].

For 122-type DMSs, we use $(Ba,K)(Zn,Mn)_2As_2$ as an example to show what μSR has achieved. The result by Zhao *et al.* is shown in Fig. 7 (adopted from Ref. [19]). The ZF-μSR time spectra of $(Ba_{0.8}K_{0.2})(Zn_{0.9}Mn_{0.1})_2As_2$ is shown in Fig. 7(a). Fast relaxation arises below the Curie temperature T_C ~ 140 K. We notice that small oscillation amplitudes exist at 5 and 20 K, which Li(Zn,Mn)As[17] and (Ga,Mn)As[23] did not exhibit. It may be caused by the domain structure and the spread of demagnetizing field. In Fig. 7(b), we show the volume fraction of magnetically ordered state deduced by the analysis of ZF and wTF μSR time spectra. It displays a similar temperature-dependence as the magnetization (inset of Fig. 7(b)), and the magnetic ordering with a full volume fraction achieved below 20 K, indicating that homogeneous and intrinsic ferromagnetism formed in this DMS[19].

4. Summary

Many other microscopic methods focusing on bulk form DMSs have also been performed. Suzuki *et al.* studied $(Ba,K)(Zn,Mn)_2As_2$ by XAS and RPES, which shows that hole carriers induced by K substitution for Ba atoms go into the As $4p$ valence band, and are weakly bound to the Mn local spins[41]. Besides, ARPES measurements suggest that Mn $3d$ and As $4p$ orbitals have strong hybridization, and impurity band is important to induce high temperature ferromagnetism in both $(Ba,K)(Zn,Mn)_2As_2$ and (Ga,Mn)As. The metallic transport may predominantly occurs in the host valence band for $(Ba,K)(Zn,Mn)_2As_2$ and in the impurity band for (Ga,Mn)As[42]. XMCD experiments indicate that As $4p$ carriers mediate the magnetization dominated by Mn of $(Ba,K)(Zn,Mn)_2As_2$. The hole doping increases the hybridization of Mn $3d$ and As $4p$ orbitals, and it promotes the exchange interactions between Mn dopants[43, 44]. Surmach *et al.* performed inelastic neutron scattering (INS) measurements on $(Ba,K)(Zn,Mn)_2As_2$. After analys-

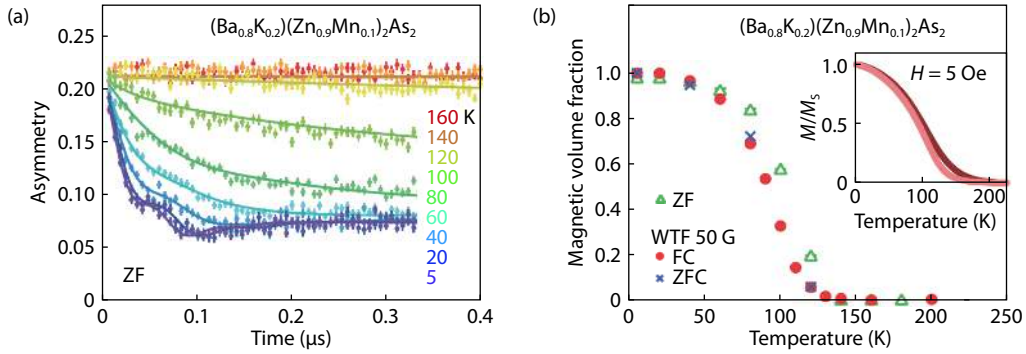

Fig. 7. (Color online) (a) ZF-μSR time spectra obtained in polycrystalline specimen of $(Ba_{0.8}K_{0.2})(Zn_{0.9}Mn_{0.1})_2As_2$. (b) Volume fraction of regions with static magnetic order, estimated by μSR measurements in ZF and WTF of 50 G. Inset: DC magnetization results of the specimens used in μSR measurements. Adopted from Ref. [19].

ing and subtracting the non-magnetic background of the intensity maps from time-of-flight neutron spectroscopy, they produced the energy spectra of INS signals for $(Ba,K)(Zn,Mn)_2As_2$. Their results indicate that the ferromagnetism may be caused by the combined action of super-exchange and double-exchange interactions[45].

In conclusion, a series of new bulk form diluted magnetic semiconductors isostructural to iron-based superconductors have been synthesized. The new DMSs have the advantage of decoupled carrier and spin doping, and bulk form is beneficial to microscopic measurements. In addition, appropriate carrier doping is beneficial to promote exchange interactions between Mn atoms and form a long range ferromagnetic ordering state, thereby improving T_C. With NMR and μSR measurements, we have shown that ferromagnetism in bulk DMSs is homogeneous and intrinsic, and they share the same ferromagnetic mechanism with the archetypal DMS (Ga,Mn)As, as summarized in Fig. 6 (adopted from Ref. [29]). Our work should help to understand the general mechanism for ferromagnetic ordering in DMSs.

Acknowledgments

The work was supported by MOST (No. 2016YFA0300402), NSF of China (No. 11574265) and the Fundamental Research Funds for the Central Universities. Authors acknowledge helpful discussions with J. H. Zhao, C. Q. Jin, Y. J. Uemura and T. Imai and the help from G. D. Morris, B. S. Hitti, and other staff in the process of μSR measurements at TRIUMF.

References

[1] Von Molnar S, Read D. New materials for semiconductor spin-electronics. Proc IEEE, 2003, 91(5), 715
[2] Matthias B T, Bozorth R M, Van Vleck J H. Ferromagnetic interaction in EuO. Phys Rev Lett, 1961, 7(5), 160
[3] Menyuk N, Dwight K, Arnott R J, et al. Ferromagnetism in $CdCr_2Se_4$ and $CdCr_2S_4$. J Appl Phys, 1966, 37(3), 1387
[4] Twardowski A, Swagten H J M, de Jonge W J M, et al. Magnetic behavior of the diluted magnetic semiconductor $Zn_{1-x}Mn_xSe$. Phys Rev B, 1987, 36(13), 7013
[5] Ferrand D, Cibert J, Wasiela A, et al. Carrier-induced ferromagnetism in p-$Zn_{1-x}Mn_xTe$. Phys Rev B, 2001, 63(8), 085201
[6] Aggarwal R L, Jasperson S N, Stankiewicz J, et al. Magnetoreflectance at the band edge in $Cd_{1-x}Mn_xSe$. Phys Rev B, 1983, 28(12), 6907
[7] Haury A, Wasiela A, Arnoult A, et al. Observation of a ferromagnetic transition induced by two-dimensional hole gas in modulation-doped CdMnTe quantum wells. Phys Rev Lett, 1997, 79(3), 511
[8] Ohno H, Shen A, Matsukura F, et al. (Ga, Mn)As: A new diluted magnetic semiconductor based on GaAs. Appl Phys Lett, 1996, 69(3), 363
[9] Ohno H. Making nonmagnetic semiconductors ferromagnetic. Science, 1998, 281(5379), 951
[10] Jungwirth T, Sinova J, Mašek J, et al. Theory of ferromagnetic (III,Mn)V semiconductors. Rev Mod Phys, 2006, 78(3), 809
[11] Dietl T. A ten-year perspective on dilute magnetic semiconductors and oxides. Nat Mater, 2010, 9(12), 965
[12] Wang M, Campion R P, Rushforth A W, et al. Achieving high curie temperature in (Ga, Mn)As. Appl Phys Lett, 2008, 93(13), 132103
[13] Chen L, Yan S, Xu P F, et al. Low-temperature magnetotransport behaviors of heavily Mn-doped (Ga, Mn)As films with high ferromagnetic transition temperature. Appl Phys Lett, 2009, 95(18), 182505
[14] Chen L, Yang X, Yang F, et al. Enhancing the Curie temperature of ferromagnetic semiconductor (Ga, Mn)As to 200 K via nanostructure engineering. Nano Lett, 2011, 11(7), 2584
[15] Tanaka M, Ohya S, Hai P N. Recent progress in III–V based ferromagnetic semiconductors: Band structure, Fermi level, and tunneling transport. Appl Phys Rev, 2014, 1(1), 011102
[16] Deng Z, Zhao K, Gu B, et al. Diluted ferromagnetic semiconductor Li(Zn, Mn)P with decoupled charge and spin doping. Phys Rev B, 2013, 88(8), 081203
[17] Deng Z, Jin C Q, Liu Q Q, et al. Li(Zn, Mn)As as a new generation ferromagnet based on a I–II–V semiconductor. Nat Commun, 2011, 2(1), 422
[18] Ding C, Man H, Qin C, et al. $(La_{1-x}Ba_x)(Zn_{1-x}Mn_x)AsO$: A two-dimensional 1111-type diluted magnetic semiconductor in bulk form. Phys Rev B, 2013, 88(4), 041102
[19] Zhao K, Deng Z, Wang X C, et al. New diluted ferromagnetic semiconductor with Curie temperature up to 180 K and isostructural to the '122' iron-based superconductors. Nat Commun, 2013, 4(1), 1442
[20] Guo S, Man H, Wang K, et al. $Ba(Zn, Co)_2As_2$: A diluted ferromagnetic semiconductor with n-type carriers and isostructural to 122 iron-based superconductors. Phys Rev B, 2019, 99(15), 155201
[21] Zhao K, Chen B, Zhao G, et al. Ferromagnetism at 230 K in $(Ba_{0:7}K_{0:3})(Zn_{0:85}Mn_{0:15})_2As_2$ diluted magnetic semiconductor. Chin Scie Bull, 2014, 59(21), 2524
[22] Guo S, Ning F L. Progress of novel diluted ferromagnetic semiconductors with decoupled spin and charge doping: Counterparts of fe-based superconductors. Chin Phys B, 2018, 27(9), 097502
[23] Dunsiger S R, Carlo J P, Goko T, et al. Spatially homogeneous ferromagnetism of (Ga, Mn)As. Nat Mater, 2010, 9(4), 299

[24] Masek J, Kudrnovsk J, Mca F, et al. Dilute moment n-type ferromagnetic semiconductor Li(Zn, Mn)As. Phys Rev Lett, 2007, 98(6), 067202

[25] Han W, Chen B J, Gu B, et al. Li(Cd, Mn)P: a new cadmium based diluted ferromagnetic semiconductor with independent spin & charge doping. Sci Rep, 2019, 9(1), 7490

[26] Wang Q, Man H, Ding C, et al. $Li_{1.1}(Zn_{1-x}Cr_x)As$: Cr doped I–II–V diluted magnetic semiconductors in bulk form. J Appl Phys, 2014, 115(8), 083917

[27] Guo S L, Zhao Y, Man H Y, et al. μSR investigation of a new diluted magnetic semiconductor Li(Zn, Mn, Cu)As with Mn and Cu codoping at the same Zn sites. J Phys: Condens Matter, 2016, 28(36), 366001

[28] Ding C, Qin C, Man H, et al. NMR investigation of the diluted magnetic semiconductor $Li(Zn_{1-x}Mn_x)P$ (x = 0.1). Phys Rev B, 2013, 88(4), 041108

[29] Ning F L, Man H, Gong X, et al. Suppression of TC by overdoped Li in the diluted ferromagnetic semiconductor $Li_{1+y}(Zn_{1-x}Mn_x)P$: A μSR investigation. Phys Rev B, 2014, 90(8), 085123

[30] Mazin I I, Singh D J, Johannes M D, et al. Unconventional superconductivity with a sign reversal in the order parameter of $LaFeAsO_{1-x}F_x$. Phys Rev Lett, 2008, 101(5), 057003

[31] Ding C, Gong X, Man H, et al. The suppression of Curie temperature by Sr doping in diluted ferromagnetic semiconductor $(La_{1-x}Sr_x)(Zn_{1-y}Mn_y)AsO$. EPL, 2014, 107(1), 17004

[32] Han W, Zhao K, Wang X, et al. Diluted ferromagnetic semiconductor (LaCa)(ZnMn)SbO isostructural to 1111 type iron pnictide superconductors. Sci Chin Phys, Mechan Astron, 2013, 56(11), 2026

[33] Chen B, Deng Z, Li W, et al. New fluoride-arsenide diluted magnetic semiconductor (Ba, K)F(Zn, Mn)As with independent spin and charge doping. Sci Rep, 2016, 6(1), 36578

[34] Yang X, Li Y, Shen C,et al. Sr and Mn co-doped LaCuSO: A wide band gap oxide diluted magnetic semiconductor with T_C around 200K. Appl Phys Lett, 2013, 103(2), 022410

[35] Guo S, Man H, Gong X, et al. $(Ba_{1-x}K_x)(Cu_{2-x}Mn_x)Se_2$: A copper-based bulk form diluted magnetic semiconductor with orthorhombic $BaCu_2S_2$-type structure. J Magn Magn Mater, 2016, 400, 295

[36] Zhao K, Chen B J, Deng Z, et al. (Ca, Na)$(Zn, Mn)_2As_2$: A new spin and charge doping decoupled diluted ferromagnetic semiconductor. J Appl Phys, 2014, 116(16), 163906

[37] Chen B, Deng Z, Li W, et al. $(Sr_{1-x}Na_x)(Cd_{1-x}Mn_x)_2As_2$: A new charge and spin doping decoupled diluted magnetic semiconductors with $CaAl_2Si_2$-type structure. J Appl Phys, 2016, 120(8), 083902

[38] Yang X, Li Y, Zhang P, et al. K and Mn co-doped $BaCd_2As_2$: A hexagonal structured bulk diluted magnetic semiconductor with large magnetoresistance. J Appl Phys, 2013, 114(22), 223905

[39] Man H, Ding C, Guo S, et al. $Ba(Zn_{1-2x}Mn_xCo_x)_2As_2$: a bulk form diluted magnetic semiconductor with n-type carriers. arXiv: 1403.4019, 2014

[40] Gu B, Maekawa S. Diluted magnetic semiconductors with narrow band gaps. Phys Rev B, 2016, 94(15), 155202

[41] Suzuki H, Zhao K, Shibata G, et al. Photoemission and x-ray absorption studies of the isostructural to Fe-based superconductors diluted magnetic semiconductor $Ba_{1-x}K_x(Zn_{1-y}Mn_y)_2As_2$. Phys Rev B, 2015, 91(14), 140401

[42] Suzuki H, Zhao G Q, Zhao K, et al. Fermi surfaces and p-d hybridization in the diluted magnetic semiconductor $Ba_{1-x}K_x(Zn_{1-y}Mn_y)_2As_2$ studied by soft X-ray angle-resolved photoemission spectroscopy. Phys Rev B, 2015, 92(23), 235120

[43] Sun F, Li N N, Chen B J, et al. Pressure effect on the magnetism of the diluted magnetic semiconductor $(Ba_{1-x}K_x)(Zn_{1-y}Mn_y)_2As_2$ with independent spin and charge doping. Physl Rev B, 2016, 93(22), 224403

[44] Sun F, Zhao G Q, Escanhoela C A, et al. Hole doping and pressure effects on the II–II–V-based diluted magnetic semiconductor $(Ba_{1-x}K_x)(Zn_{1-y}Mn_y)_2As_2$. Phys Rev B, 2017, 95(9), 094412

[45] Surmach M A, Chen B J, Deng Z, et al. Weak doping dependence of the antiferromagnetic coupling between nearest-neighbor Mn^{2+} spins in $(Ba_{1-x}K_x)(Zn_{1-y}Mn_y)_2As_2$. Phys Rev B, 2018, 97(10), 104418